Bull. Disas. Prev. Res. Inst., Kyoto Univ., Vol. 23, Parts 3-4, No. 214, December, 1973

An Experiment of Steel Reinforced Concrete Cruciform Frames

By Minoru WAKABAYASHI, Takeshi NAKAMURA and Shosuke MORINO

(Manuscript received December 25, 1973)

Abstract

An experimental study is carried out on the behavior of steel reinforced concrete beam-to-column assemblages subjected to constant vertical and repeated horizontal loads. The effects of the depth of H-steel cross section, the ratio of the flexural strength of H-steel to the total flexural strength of the steel reinforced concrete cross section and the vertical load on the behavior of the specimens failing in the flexure in the column or in the shear in the connection panel are investigated.

1. Introduction

The experimental study presented in this paper was planned to investigate the elastic-plastic hysteretic behavior of precast steel reinforced concrete beam-and-column assemblages, which have been frequently used in the recent practice of the prefabricated construction of building structures. In the usual prefabricated beam-to-column connections, the most general construction pattern would be the combination of the steel reinforced concrete columns and steel concrete or pure steel beams. The detail of the steel beam-to-column connection requires the thicker concrete cover of the column, and sometimes the ratio of the depth of the steel portion of the column to the total column depth becomes 1/3. In addition to this tendency, from the economical point of view, the larger fraction of the total bending moment capacity of the column tends to be shared by the reinforced concrete portion rather than by the steel portion of the column. Under these circumstances, a rather unbalanced proportioning of the steel portions of the column and the beam is frequently encountered, and some problems arise; Does the maximum flexural strength computed by the so-called method of superposition for such a column with a thick concrete cover really develop? Does the undesired strength deterioration occur in the process of repeated loading? What percentage of the total shear strength of the panel can be carried by concrete? Probably the most critical question may be whether the proper stress transmission could be anticipated in the panel zone consisting of the unbalanced combination of steel portions of the column and the beam.

To obtain the answers to the questions stated above, planned was a series of tests on steel reinforced concrete beam-and-column assemblages under constant vertical and repeated horizontal loads, with the experimental parameters being the ratio of the flexural strength of steel portion to the total column strength, the magnitude of the vertical load on the column, depth of H-steel portion in the column and the failure mechanism, i.e., the flexural failure of the column or the shear failure of the connection panel.

2. Tests

2.1 Test Specimen

Twelve cruciformed steel reinforced and ordinary reinforced concrete specimens are characterized by 4 testing parameters as shown in Table 1; the flexural strength

Table 1 Characteristics of specimens

	Flexural Ratio	H-Steel Cross Section (mm)	Flexural Failure	Shear Failure
Steel Reinforced Concrete Column	0.8	300 × 100	F1, F2	S1
		250 × 100	F3, F4	S2
		200 × 100	F5	
	0.4	300 × 90	F6	S3
		250 × 100	F7	
Reinforced Concrete Column	0	0	R1*, R2*	

* Actually bond failure occurs.

ratio, failure mechanism, depth of the H-steel section in the column and the magnitude of axial load, where the flexural strength ratio is the ratio of the full plastic moment of the built-up H-steel section to the flexural strength of the total column cross section under pure bending. The following values and types are selected for each of the above described testing parameters.

Flexural strength ratio: 0.8, 0.4 and 0.

Depth of H-steel section: 300, 250 and 200 millimeters.
(ratio to the depth of total cross section) (2/3) (5/9) (4/9)

Failure mechanism: flexural failure of the column cross section and shear failure of the connection panel.

Axial load: 70 and 140 tons.

The following design considerations are given to each of the specimen.

1. Column cross section of each specimen is so designed to have approximately constant value of the maximum flexural strength, computed for the zero axial load case by the superposition of the contributions from each component parts; steel, reinforcing bars and concrete.
2. Each specimen is so designed to fail either in the flexure in the column cross section or in the shear in the connection panel.
3. Column cross section is either of steel reinforced concrete or of ordinary reinforced concrete. Beam cross section consists of H-steel encased in concrete. The face of one flange of H-steel cross section is not covered by concrete*1.

*1: Bare flange style is frequently used in the prefabricated construction practice. Studs or other type shear connectors to connect prefabricated slab plates will be eventually welded on the bare flange face.

4. In order to aviod the shear failure in the column and the shear and flexural failures in the beam, amount of stirrups in the column and thicknesses of flange and web plates of the beam are sufficiently large*2.

The characteristics of each specimen are tabulated in Table 1, from which testing parameters controlling each specimen can be read. In Fig. 1, the cross sectional

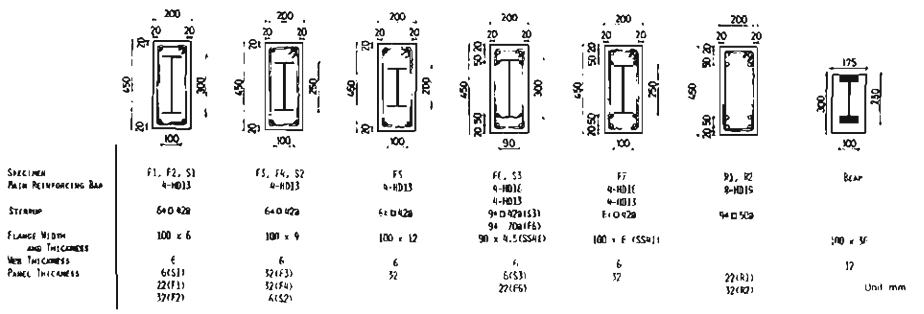

Fig. 1. Cross sections of columns and a beam.

proportions of beams and columns of twelve specimens are shown. H-steel section is built-up from the plates with specified thicknesses. Both ends of main reinforcing bars are welded to the steel end plates. Beam cross section is identical for all of 12 specimens. Thickness of concrete cover is commonly 2 cm, measured from the outside face of stirrups. Center-to-center distance between the main reinforcing bars in the first and second rows is 5 cm if necessary.

Dimensions of the cruciform specimen is shown in Fig. 2, which are common for

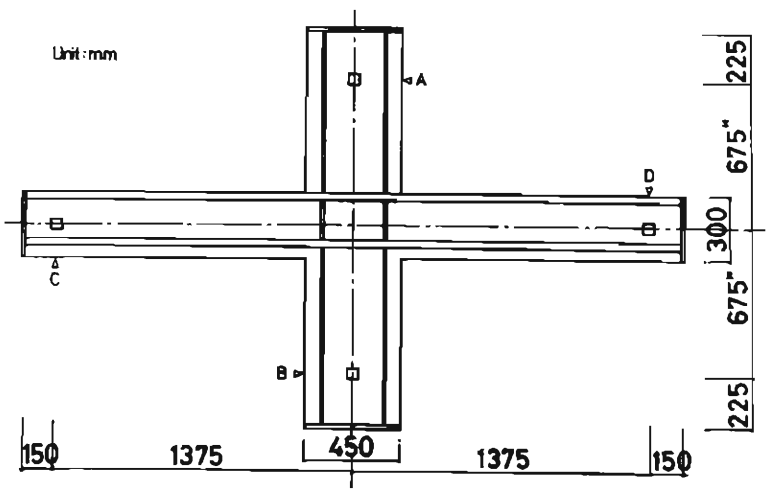

Fig. 2. Size of specimen.

*2: In specimens R1 and R2, spacing of stirrups to prevent the shear failure in the column is too small. Column lengths of these two specimens are thus increased to about twice the column length of others.

all specimens except specimens R1 and R2. Column length of these two specimens is 1200 mm instead of 675 mm for the others (marked with an asterisk in Fig. 2). Points A, B, C and D are supporting points of the columns and loading points on the beams, respectively. Steel portion of each specimen is built up by groove welding columns to the single member of the beam.

2.2 Loading System

Figure 3 shows the loading set-up schematically. Whole view of the test is shown in Photo. 1. Constant vertical load is applied by 200 ton hydraulic jack(marked

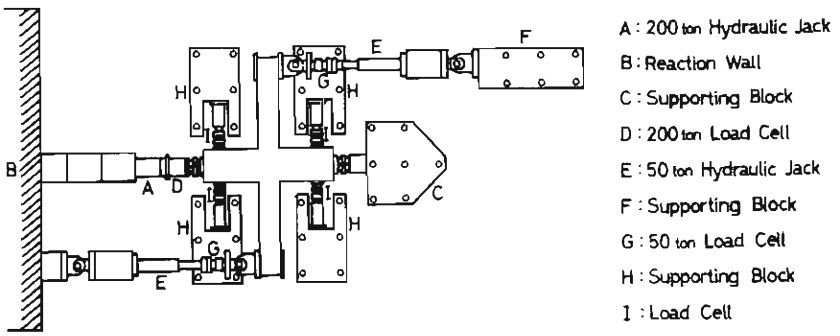

Fig. 3. Loading system.

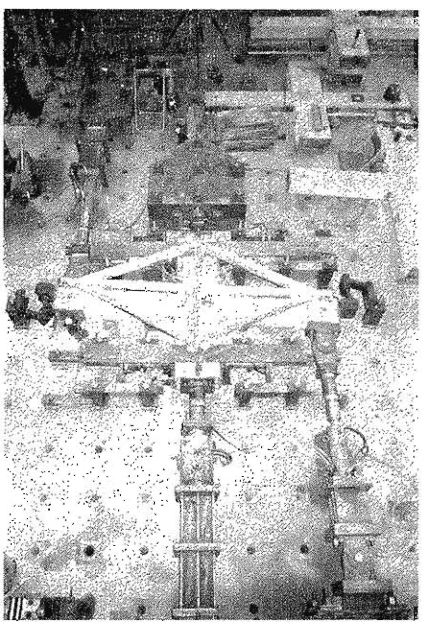

Photo. 1. Test set -up.

A in Fig. 3), and its reaction is carried by the reaction wall (B) and the supporting

block (C). The magnitude of the vertical load is measured by 200 ton load cell (D). Alternately repeated horizontal loads are applied at the beam tips simultaneously by two 50 ton push-pull type hydraulic jacks (E). and their reactions are supported by the wall and the block (F). The magnitudes of the horizontal loads are measured by 50 ton tension-compression load cells (G). The horizontal reactions at the column ends are carried by the supporting blocks (H) and measured by the load cells (I).

Each of the supporting blocks is fixed to the test bed by steel tendons for prestressed concrete construction with 33 mm diameter (tensile force: 60 tons). Hydraulic jacks and load cells for the horizontal loading are sandwiched by two pins, and they allow the movement of the specimen in the direction perpendicular to the axis of the horizontal load application. The out-of-plane movements at both beam tips are prevented by "caterpillar" type lateral buckling preventers (Photo. 2). End supports for the column are supplied by the combination of ball and roller bearings, as shown in Fig. 4.

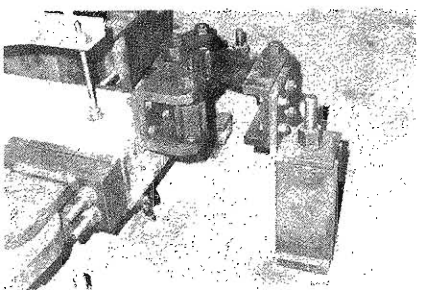

Photo. 2. Lateral buckling preventer.

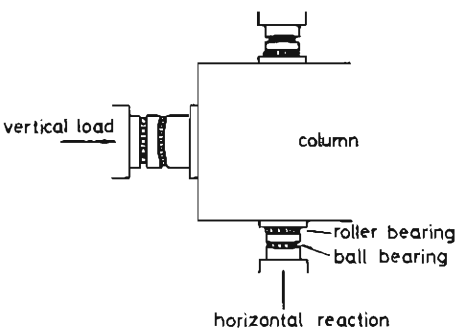

Fig. 4. Supporting system at column end.

Figure 5 shows a typical loading program for the repeated horizontal load. First, the prescribed magnitude of the vertical load is applied on the column of the specimen, and it is kept constant during the test. The specimen then experiences ± 10 tons of the horizontal loads applied at the beam tips as the first cycle of the horizontal loading. From the second cycle, the loading is so controlled that the amplitude of the chord rotation angle*3 of the column be the prescribed value as shown in Fig. 5; 0.01, 0.02, 0.03, 0.04. At each amplitude, two cycles of loading are applied

*3: See section 2.3.

on the specimen, and hence 9 cycles of loading are specified. F2 and F4 are subjected to 140 ton axial load, and others are subjected to 70 tons.

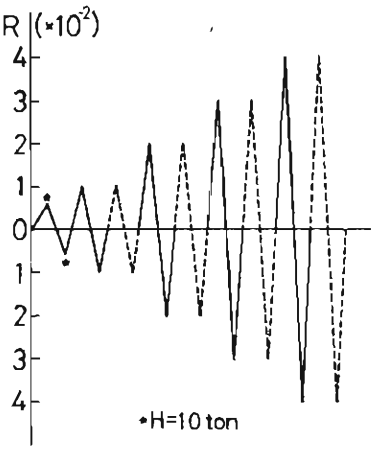

Fig. 5. Loading Program.

2.3 Data

Displacements and strains occurring in the specimen are detected by dial gauges and wire strain gauges, respectively. Figures 6(a) and (b) show the displacement

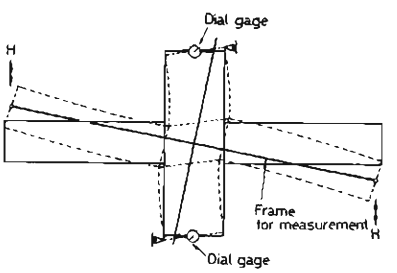

(a)

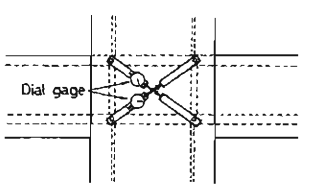

(b)

Fig. 6. Displacement detection system.

detection system. Horizontal displacements at column ends are measured by two dial gauges in Fig. 6(a), as movements at the two tips of the one bar of the cruciformed measuring frame, the other two bar ends of which are fixed to the specimen by bolts encased in the beams at the points of the horizontal load application. Two dial gauges are placed on the columns at the points of the horizontal reaction. Column displacement δ is given by the formula

$$\delta = \frac{\Delta^1 + \Delta^2}{2} \tag{1}$$

where Δ^1 and Δ^2 are data detected by two dial gagues in Fig. 6(a). The chord rotation angle R of the column is given by

$$R = \frac{\delta}{L} \tag{2}$$

where L is the column length, and 1200 mm for specimens R1 and R2 and 675 mm for all other specimens should be taken.

Two dial gauges in Fig. 6(b) are used for measuring length changes of two diagonals*4 of the panel zone rectangle. The shear deformation angle γ of the connection panel is given by the formula

$$\gamma = \frac{\Delta^3 - \Delta^4}{2} \cdot \frac{\sqrt{a^2 + b^2}}{ab} \tag{3}$$

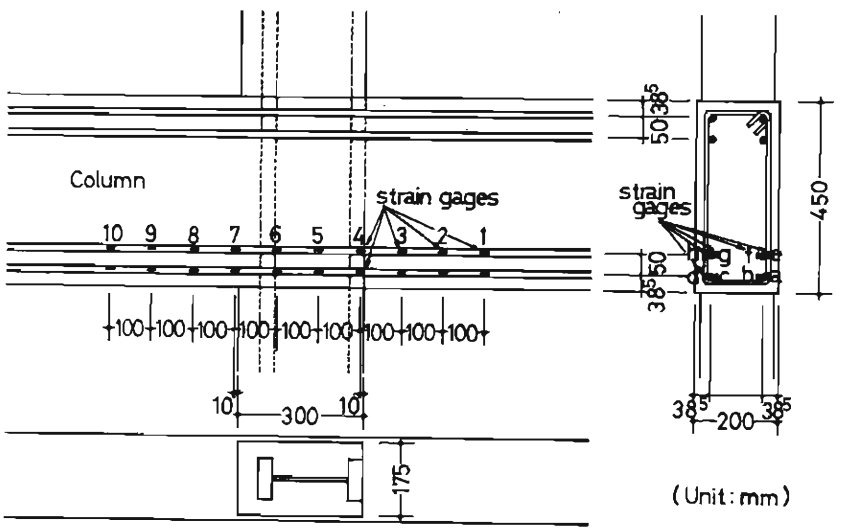

Fig. 7. Locations of strain gauges on reinforcing bars.

*4: Length of the diagonals means the diagonal distance between two bolts welded to the steel portion at intersecting points of center lines of beam flanges and rib plates.

where Δ^3 and Δ^4 are detected data by two dial gauges, and a and b are lengths of sides of the panel rectangle. The measured values of a and b are shown in Table 5.

The longitudinal strains occurring in beams and columns, and strains in the connection panel are detected from the wire strain gauges mounted on concrete face and steel flanges of the beams and columns, and rosette gauges mounted on the concrete and steel panel zones. The most important observations are made from the strain data obtained from a set of the wire strain gauges mounted on the main reinforcing bars of specimen R2 with 10 cm interval. This is to investigate the strength reduction caused by the slip of the reinforcing bars occurring around the connection panel. Exact locations of the wire strain gauges for this purpose are shown in Fig. 7.

3. Test Results

3.1 Mechanical Properties of Materials

Mechanical properties obtained from the cylinder test for concrete and the tension tests for the reinforcing bars and the steel plates are tabulated in Tables 2, 3 and 4, respectively.

The weight ratio among cement, sand and gravel for the used concrete is 1 : 2.97 : 3.25, and water-cement ratio is 58%. The result of the slump test is 10 cm. Four

Table 2. Concrete strength.

Specimen	Compressive Strength (kg/cm^2)	Tensile Strength (kg/cm^2)
F1	312.3	26.3
F2	380.8	28.7
F3	373.6	30.6
F4	384.2	28.8
F5	388.8	31.7
F6	340.8	28.7
F7	386.7	32.0
S1	316.7	27.5
S2	349.9	29.2
S3	330.9	25.0
R1	241.1	21.7
R2	342.5	32.1

or three out of 6 cylinders are supplied to determine the compressive cylinder strength F_c, and the other two or three are for the splitting tensile tests. The main tests of cruciform specimens are done after a week to 5 weeks have passed from the time of concrete casting. Cylinder tests are carried out in the same day as the corresponding main tests.

Two tension test specimens are taken from each of main reinforcing bars and stirrups of each cruciform specimen, and mean values of test results are tabulated in Table 3. As for the steel plates, 3 tension test specimens are prepared for each thickness of the plates involved in the cruciform specimens. Mean values of the mechanical properties are agian shown in Table 4.

Table 3. Mechanical properties of reinforcing bars.

	Specimen	Size*1 (mm)	Area*1 (cm^2)	Yield Stress (t/cm^2)	Maximum Stress (t/cm^2)	Maximum Elongation (%)
Main*2 Reinforcing Bars	F1	D13	1.27	3.769	5.878	20.7
	F2	D13	1.27	3.894	5.898	20.1
	F3	D13	1.27	3.833	5.906	19.1
	F4	D13	1.27	3.852	5.890	19.8
	F5	D13	1.27	3.860	5.928	19.5
	F6	D16	1.99	4.186	6.015	20.4
		D13	1.27	3.715	5.776	20.4
	F7	D16	1.99	3.637	5.503	23.5
		D13	1.27	3.882	5.869	19.4
	S1	D13	1.27	3.791	5.909	20.8
	S2	D13	1.27	3.870	5.914	20.1
	S3	D16	1.99	4.180	6.013	23.1
		D13	1.27	3.801	5.854	20.3
	R1	D19	2.87	3.800	5.904	21.5
	R2	D19	2.87	3.950	5.791	23.5
Stirrups*3	F1, S1, S3	6	0.28	6.929	7.643	6.7
	F6, R1	9	0.94	3.531	4.688	6.0
	F2, F3, F4, F5, F7, S2	6	0.28	6.098	6.586	9.5
	R2	9	0.94	2.282	3.150	26.5

Note: *1 Nominal size used.
*2 Material is SD35.
*3 Material is SR24 or equivalent.

Table 4. Mechanical properties of steel plates.

Specimen	Plate	Thickness*1 (mm)	Yield Stress (t/cm^2)	Maximum Stress (t/cm^2)	Maximum Elongation (%)
F1	Flange	6	3.923	5.480	28.6
	Web	6	3.923	5.480	28.6
	Panel	22	3.317	5.377	32.8
F2	Flange	6	3.916	5.493	26.4
	Web	6	3.916	5.493	26.4
	Panel	32	3.130	5.094	33.1
F3	Flange	9	3.294	5.204	29.8
	Web	6	3.916	5.493	26.4
	Panel	32	3.130	5.094	33.1
F4	Flange	9	3.294	5.204	29.8
	Web	6	3.916	5.493	26.4
	Panel	32	3.130	5.094	33.1
F5	Flange	12	3.711	5.513	28.8
	Web	6	3.916	5.493	26.4
	Panel	32	3.130	5.094	33.1
F6	Flange	4.5*2	2.483	4.020	35.6
	Web	6	3.923	5.480	28.6
	Panel	22	3.317	5.377	32.8
F7	Flange	6*2	3.563	4.685	28.8
	Web	6	3.916	5.493	26.4
	Panel	32	3.130	5.094	33.1

Table 4. Mechanical properties of steel plates plates (continued)

Specimen	Plate	Thickness*1 (mm)	Yield Stress (t/cm^2)	Maximum Stress (t/cm^2)	Maximum Elongation (%)
S1	Flange	6	3.923	5.480	28.6
	Web	6	3.923	5.480	28.6
	Panel	6	3.923	5.480	28.6
S2	Flange	9	3.294	5.204	29.8
	Web	6	3.916	5.493	26.4
	Panel	6	3.916	5.493	26.4
S3	Flange	4.5*2	2.483	4.020	35.6
	Web	6	3.923	5.480	28.6
	Panel	6	3.923	5.480	28.6
Beam: F1, F6, S1, S3, R1	Flange	36	3.443	5.319	37.1
	Web	12	3.610	5.332	28.6
Beam: F2, F3, F4, F5, F7, S2, R2	Flange	36	2.817	4.818	37.5
	Web	12	3.711	5.513	28.8

Note *1 Nominal size used.
*2 Material used is SS41, and all others are SM50.

3.2 Horizontal Load-Displacement (Chord Rotation Angle) Curve

The hysteretic relationships between the horizontal load H and the column displacement δ or the column's chord rotation angle R are shown in Figs. 8 (a) to (l). In these figures, the first hysteresis loop obtained under each displacement amplitude is plotted by a solid line, and the second one by a dashed line.

The following general observations may be derived from the comparison of hysteresis loops.

1. Specimens with steel reinforced concrete columns under 70 ton vertical load: The imaginary load-displacement curve obtained by connecting the origin and turning points on the hysteresis loops obtained in the first loading cycle under each displacement amplitude, shows clear unloading in case of shear failing specimens, S1 and S3, while that shows a rather long plateau in case of the flexural failing specimen, F1*5.

   However, this experimental observation is reversed for specimens F3 and S2. This unloading portion can be more or less observed for specimens F5 and F7, although they fail in the flexure of the columns.

   As a whole, the strength deterioration observed in the second loading cycle at each displacement amplitude is small except for specimen F7. Specimen F7, which has the second smallest depth of the H-steel cross section and the flexural ratio of 0.4, shows quite large strength deterioration in the second

*5: As a matter of fact, in case of F6, the breakage occurring at the welded end of the column steel to the beam (see Photo. 3) caused a rapid unloading when the chord rotation angle is reaching 0.03 radian. However, supposing this breakage would not have occurred, it would be expected that the above statement is true also for F6.

cycle, and this deterioration becomes larger as the displacement amplitude increases.

In general, hysteresis loops of the flexure failing specimens are spindle shaped, while the shear failing specimens show slightly thinner hysteresis loops.

2. Specimens with ordinary reinforced concrete columns: The hysteretic behaviors of specimens R1 and R2 are quite different from others explained above. The imaginary load-displacement curve obtained by connecting turning points shows very steep unloading curve. In addition, the strength deterioration in the second loading cycle under each displacement amplitude is quite severe, and the energy dissipation could not be much expected in the second loading cycles. Each of hysteresis loops becomes very thin compared with those of specimens with steel reinforced concrete columns.
3. Specimens under 140 ton vertical load: Specimens F2 and F4 are subjected to twice as large vertical load as others. Otherwise the proportioning for these two specimens is identical to specimen F1*[6] and F3, respectively. The effect of the vertical load clearly appears as the phenomena such as the undesirably large strength deterioration with the increase of the displacement amplitude, and the small deformation capacity. The test is terminated when the connection panel portion sticks out in the direction perpendicular to the plane of the specimen, caused by the large vertical load.

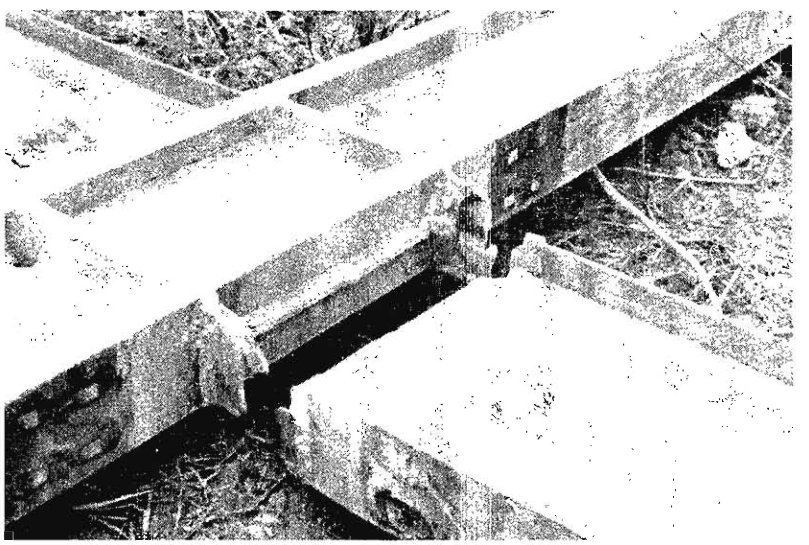

Photo. 3. Breakage of welded column end.

*6: The thickness of the steel plate in the connection panel of F2 is larger than that of F1.

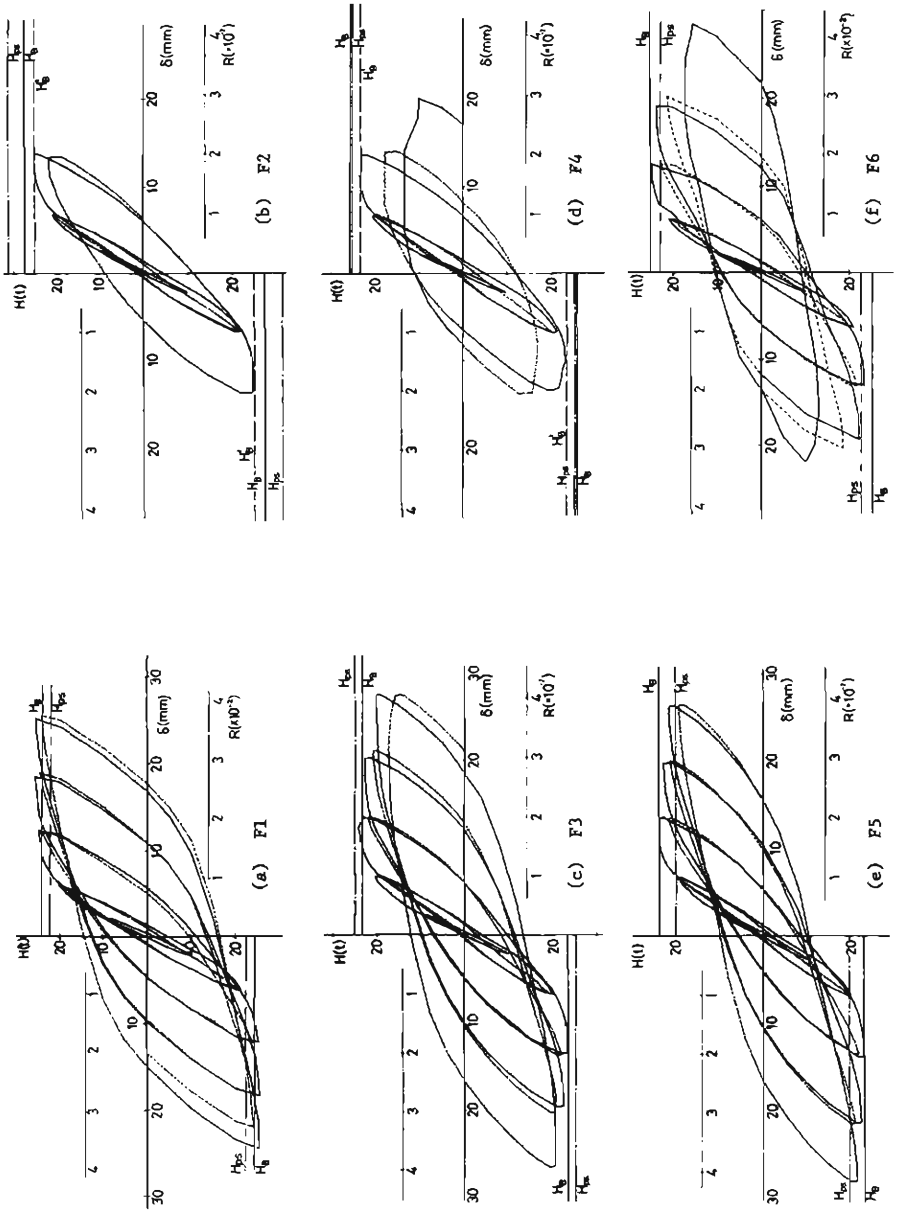

Fig. 8. Horizontal load-displacement relations.

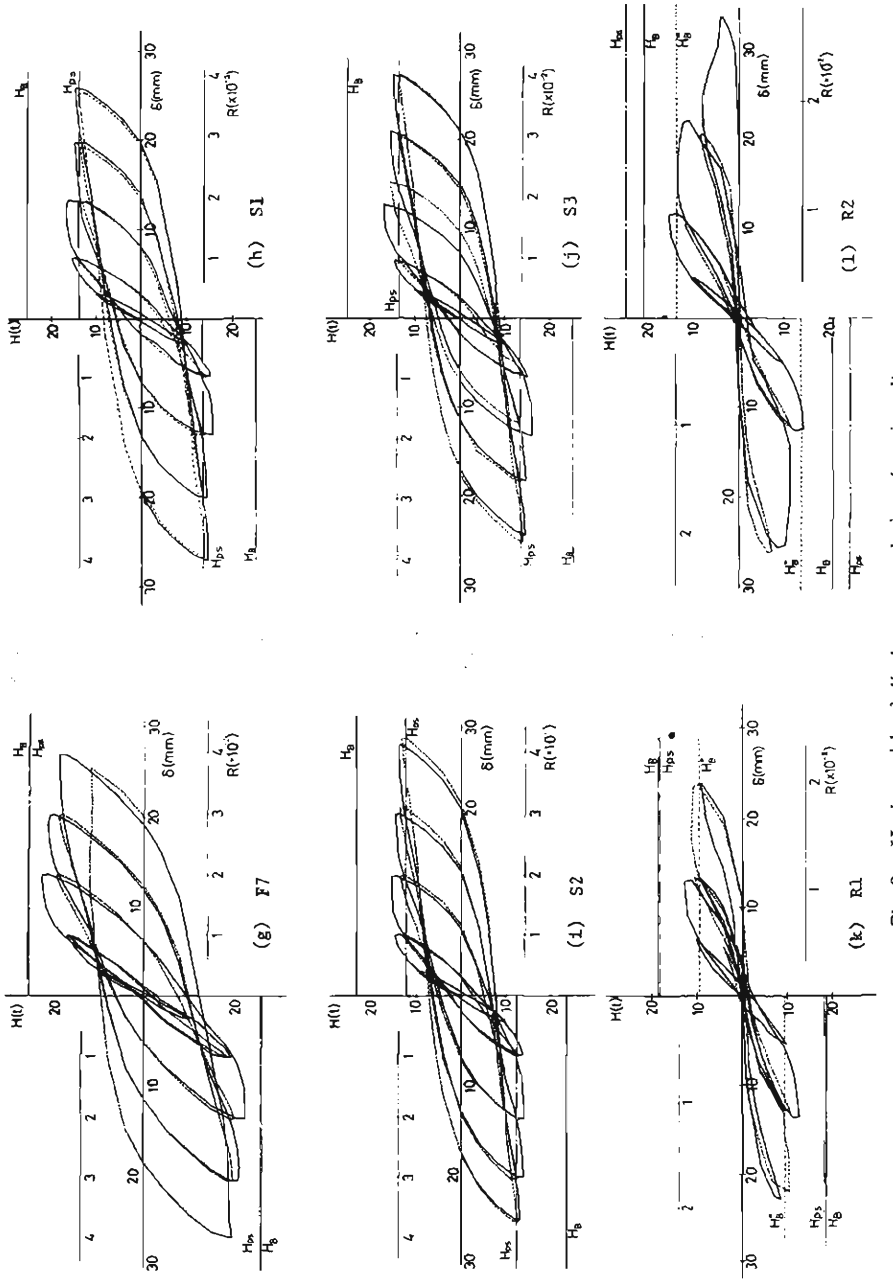

Fig. 8. Horizontal load-displacement relations (continued).

3.3 Horizontal Load- Shear Deformation Curve

Figures 9 (a) to (l) show the hysteretic relationships between the horizontal load H and the shear deformation angle γ in the connection panel, in which the hysteresis loop obtained in the first loading cycle under each displacement amplitude is shown by a solid line and that in the second is shown by a dashed line. These experimental results are all deduced from the dial gauge data.

Some parts of the hysteresis loops indicate the unrealistic dial gauge data. This

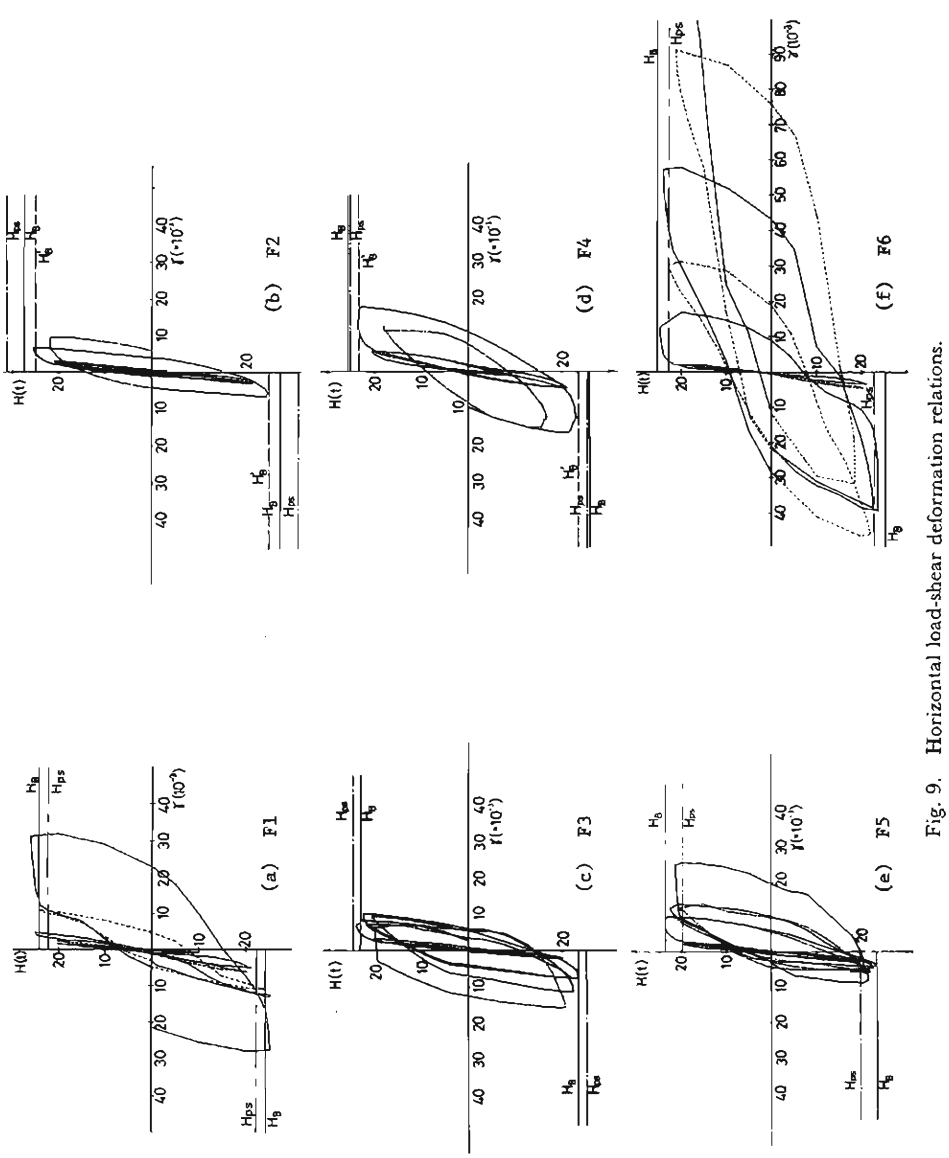

Fig. 9. Horizontal load-shear deformation relations.

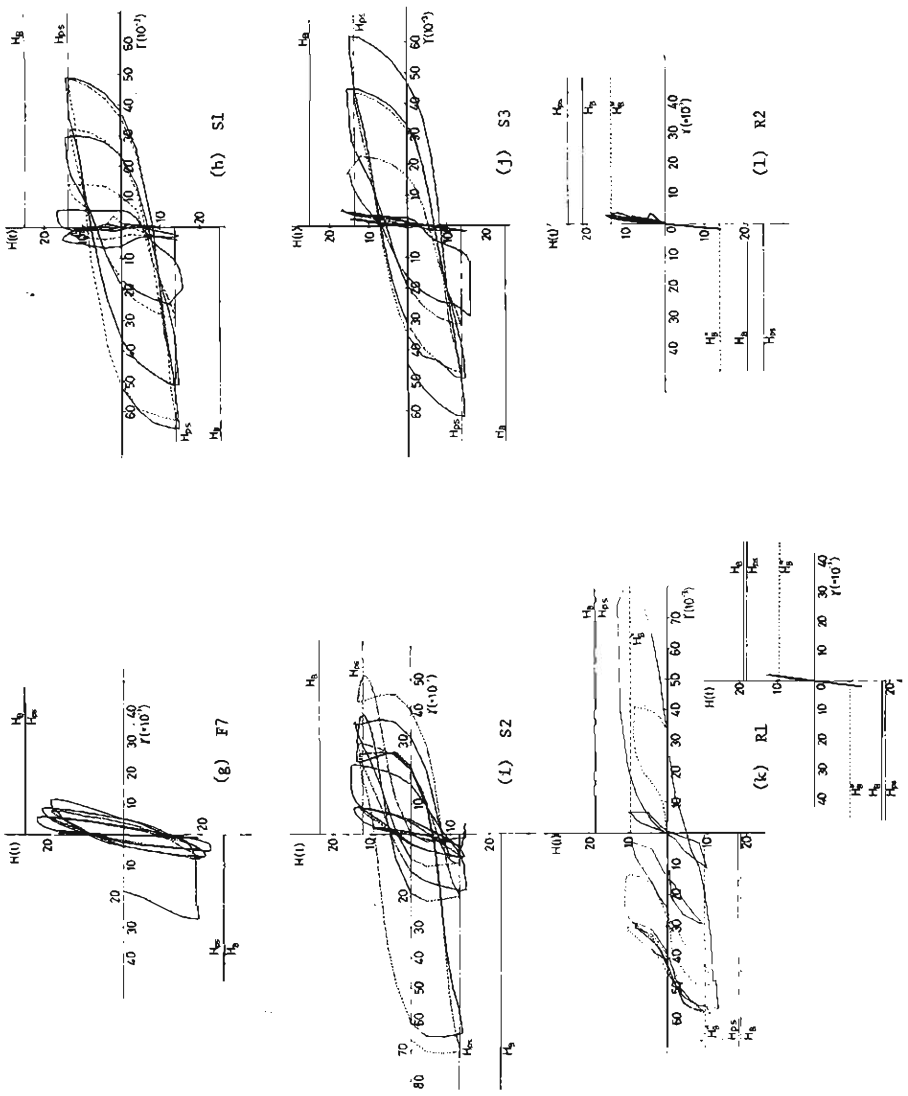

Fig. 9. Horizontal load-shear deformation relations (continued).

is considered as a result of the prevention of free and smooth movement of the bolts supporting the dial gauges caused by broken concrete fragments in the connection panel zone. However, the following observations may be available:

The shear deformation angle in the connection panel of the shear failing specimens constantly increases with the increase of the displacement amplitude controlling the loading hystory. On the other hand, that of the flexural failing specimen increases to about 0.01 when 3 cycles of loading are terminated. The increase of the shear deformation angle caused by the subsequent loading is not very large*7. Although

*7: This statement is not true for specimen F6. Rather large shear deformation observed in this specimen may be related to the breakage of the welded column end, but a reasonable explanation could not yet be given.

the final failure of the specimen is due to the flexural failure of the column, the connection panel does not necessarily remain in the elastic range, and yielding in the steel panel plate and crack propagation in the concrete panel can be observed.

The test result of specimen R1 is rather unreliable, and hence H–γ curve computed from the rosette gauge data of the steel panel plate is shown in the lower right figure in Fig 9 (k), to understand that the connection panel does not fail.

3.4 Crack Observation

The crack patterns around the connection panel at the final state of the test are shown in Figs. 10 (a) to (l). To simplify the description of the crack initiation and propagation, let us call the first half of the hysteresis loop obtained in the Nth cycle of loading as $N/2$, and the second half as $2N/2$.

The crack patterns at the final state of the test observed from those figures seem very similar for all specimens. However, the patterns of the crack initiation and growing clearly show the difference of the failure mechanism of each specimen.

For all specimens, the bending crack first appears on the beam during 1/2 cycle of loading, since no reinforcing bar is provided to the beam.

As for the flexure failing specimens (excluding R1 and R2, which will be clarified later to fail in the slip of the main reinforcing bars), the bending cracks on the column initiate from several different locations during 1/2 to 3/2 cycles of loading, and they keep growing to become shear cracks on the column in the subsequent loading. At the same time or later, the cracks along the main reinforcing bars or the steel flanges in the column appear, and they also keep growing. The shear cracks in the panel zone also appears nearly at the same time as, but not before, the bending cracks. However, they do not grow much until the specimen reaches its final state. In specimens F2, F3, F4 and F5, the appearance of the shear cracks in the panel is quite late (at 4/2 or 7/2 cycle of loading).

In case of the shear failing specimens, on the contrary, the shear cracks in the panel grow more rapidly than the bending cracks in the column, although they appear almost simultaneously at 1/2 to 3/2 cycles of loading. The initiation of the cracks along the main reinforcing bars is delayed to 7/2 cycles of loading.

Regardless of the failure mechanism, the concrete at the flexural compression side of the column end begins to crash after 5/2 to 11/2 cycles of loading, and then the crashed concrete fragments drop down from the compression side of the column and also from the panel zone. At the very end of the test, the main reinforcing bar in the panel zone buckles out of the concrete cover, and the out-of-plane deformation and torsional deformation of the column are observed in some specimens.

For specimens under 140 ton vertical load, which are both designed to fail in the flexure of the column, more or less the same crack pattern as described above is observed. The initiation of the cracks along the main reinforcing bars, the drop down of the crashed concrete fragments, the buckling of the main reinforcing bars and the out-of-plane deformation of the specimen, occur a little earlier than in the case of specimens under 70 ton vertical load. Both tests are terminated when it becomes impossible to keep the prescribed vertical load (140 tons) constant during the application of the horizontal load.

Characteristics of the specimen with ordinary reinforced concrete columns lie

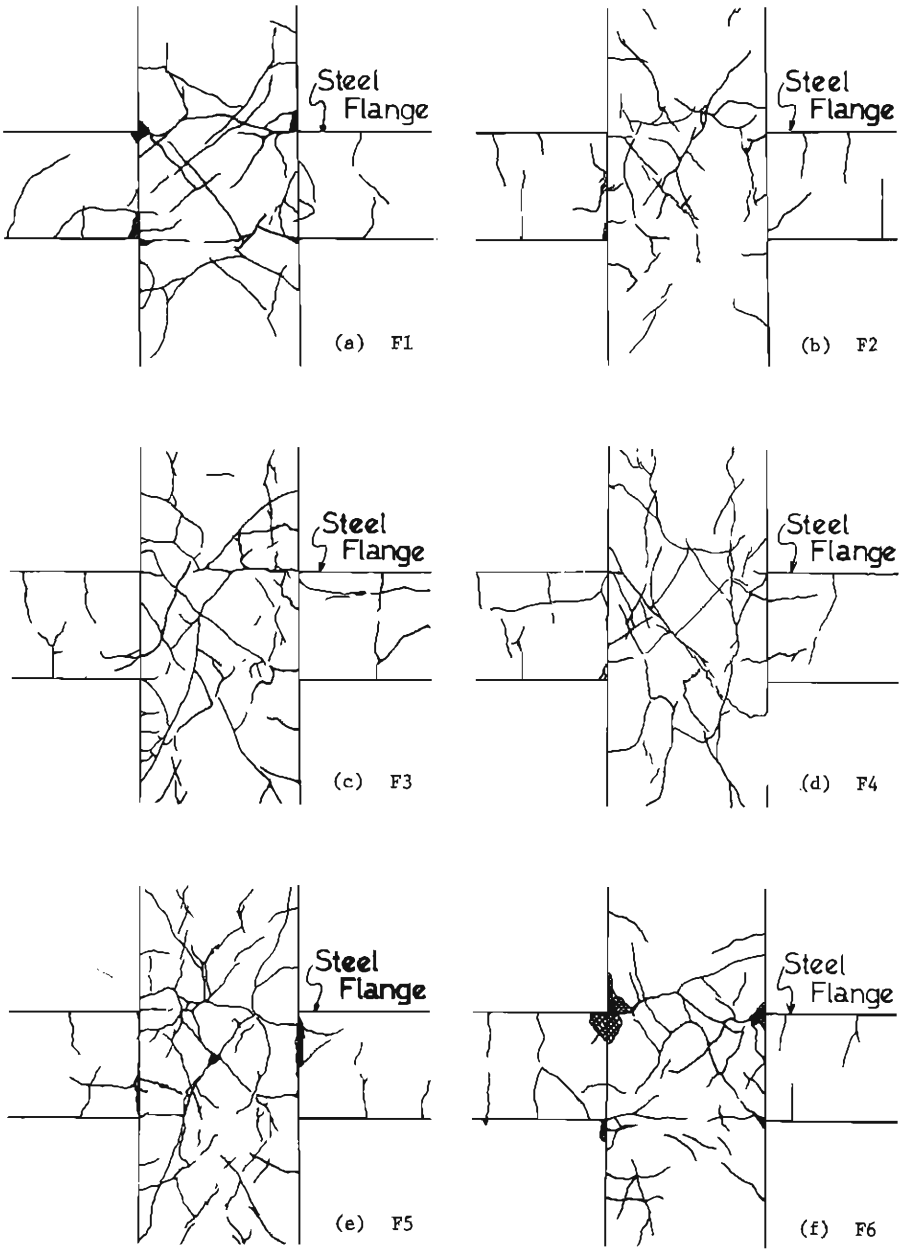

Fig. 10. Crack patterns.

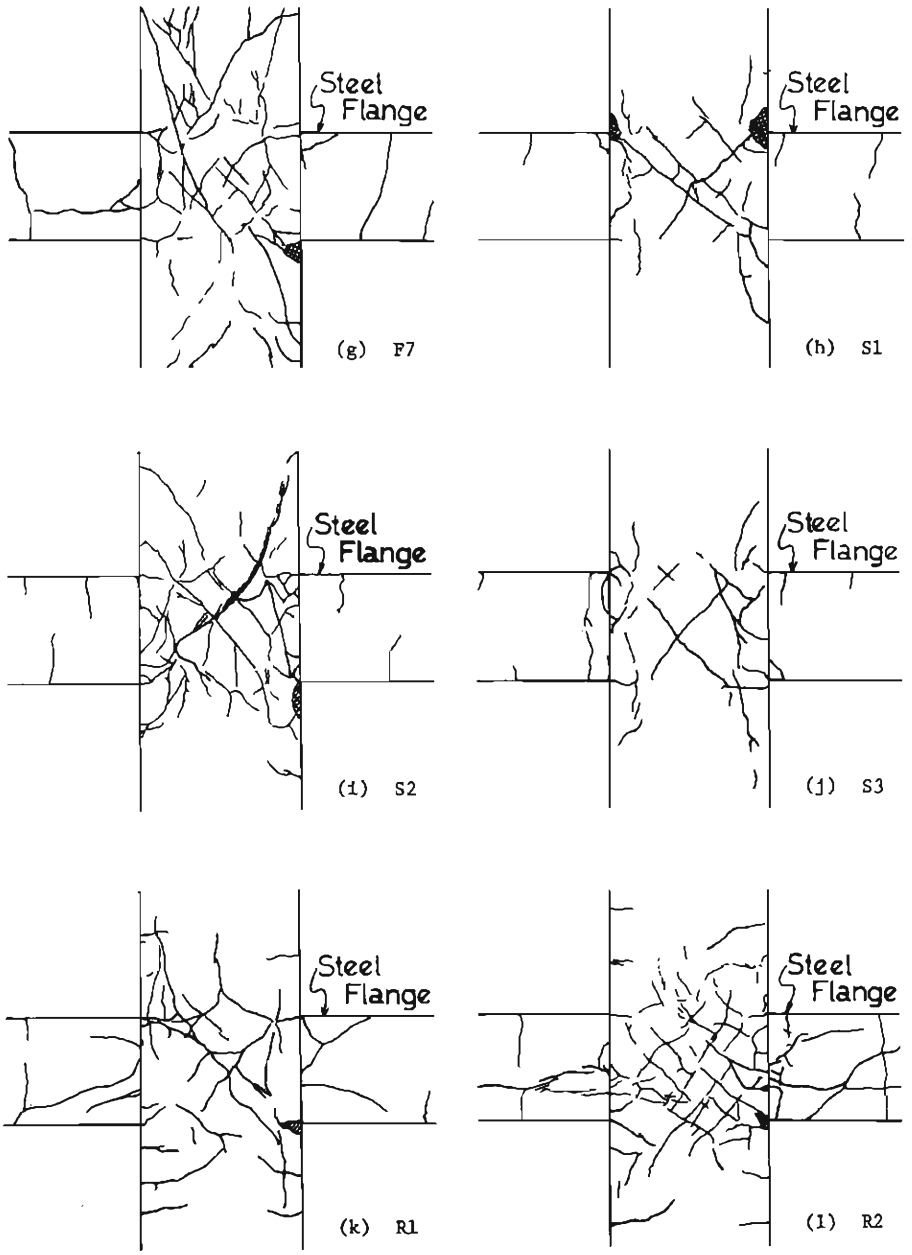

Fig. 10. Crack patterns (continued).

in the process of rapid growing of the cracks along the main reinforcing bars, which appear during 2/2 to 3/2 cycles of loading. The shear cracks in the connection panel do not appear until 4/2 to 7/2 cycles of loading. The buckling of the main reinforcing bars and the out-of-plane deformation are not observed.

4. Computation for the Maximum Load Carrying Capacity

The maximum load carrying capacity of each specimen may be computed from the maximum flexural strength of the column cross section or from the maximum shear strength of the connection panel, according to the design conditions for each specimen.

The maximum flexural strength of the column cross section can be obtained by two approaches. The one is the so-called "method of superposition", which sums up the bending moment M — axial force N interactions for each component part; concrete, steel and reinforcing bars. Each interaction is independently obtained. Strictly speaking, this method violates the strain compatibility which is resulted from the assumption that the plane remains the plane after the deformation occurs. Then, the other approach, which is the so-called "method of ultimate strength", is also possible, in which the strain compatibility is considered.

As for the computation of the maximum shear strength of the connection panel, the method of superposition is employed, in other words, it is assumed that the maximum shear strength is given as the sum of the contributions from the steel panel and concrete panel computed independently. Derivation of the equations shown in this chapter is quite lengthy, and thus only the final versions of the necessary equations are shown. The readers may refer to Refs. 1 and 2.

4.1 Assumptions

Compressive stress-strain curve of concrete is assumed to be given by a parabola

$$\frac{\sigma_C}{\sigma_B}=2\cdot\frac{\varepsilon_C}{\varepsilon_B}-\left(\frac{\varepsilon_C}{\varepsilon_B}\right)^2 \tag{4}$$

and a straight line connecting $(\varepsilon_B, \sigma_B)$ and $\{(1+\kappa)\varepsilon_B, 0.75\sigma_B\}$, where

σ_C: concrete stress
ε_C: concrete strain
σ_B: maximum concrete strength
ε_B: concrete strain corresponding to σ_B
κ: a parameter determining the limit of the concrete strain

This relation is plotted in Fig. 11. In the actual computation, it is assumed that $\varepsilon_B=0.0015$ and $\kappa=1$. The maximum concrete strength σ_B is computed from

$$\sigma_B=F_C\cdot\left(0.85-2.5\frac{A_C}{B\cdot D}\right) \tag{5}$$

where

F_C: cylinder strength of concrete
A_C: area of flange and main reinforcing bars in the compression side
B, D: width and depth of the cross section, respectively

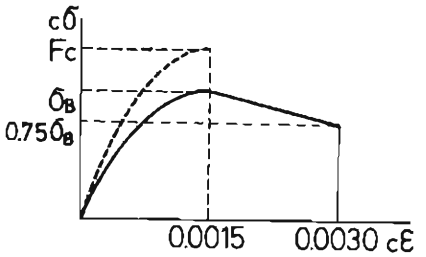

Fig. 11. Stress-strain relation of concrete.

Concrete is assumed to provide no tensile strength.

For steel elements and main reinforcing bars, the stress-strain relationships are assumed to be ideal elastic-perfectly plastic, and Young's modulus for both of them is assumed to be identically 2.1×10^3 t/cm²*8.

It is assumed that the total cross section containing concrete, H-steel and the main reinforcing bars is entirely doubly symmetrical as shown in Fig. 12, and that two flanges and all reinforcing bars have their common yield stress levels, respectively. In Fig. 12,

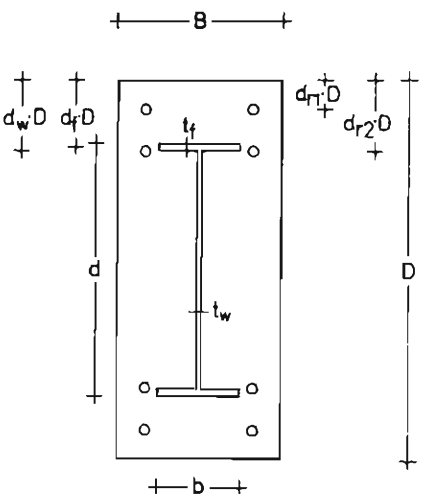

Fig. 12. Cross section of a column.

B: width of cross section
D: depth of cross section
b: steel flange width
d: H-steel depth
t_f: flange thickness

*8: Young's modulus for the deformed bar obtained from the results of tension test and the nominal area is quite different from this value. The real value, 1.736×10^3 t/cm², is used only when the analysis considering the slip of the reinforcing bars is carried out.

$d_{r1}D$, $d_{r2}D$: distances between the extreme fiber and the gravity center of reinforcing bars in the first and second rows, respectively.

d_fD, d_wD: distances between the extreme fiber and the gravity center of the flange, and the extreme fiber of the web, respectively.

It should be noted that the compression is positive and tension is negative in the following discussion.

4.2 Maximum Flexural Strength of the Cross Section — Method of Superposition

a. *M–N* Interaction of Concrete

Taking the neutral axis ratio k as an independent variable, the axial force N_c (positive in compression) and bending moment M_c carried by concrete can be given by the formulas

$$\left.\begin{aligned} N_C &= \frac{16+21\kappa}{24(1+\kappa)} BD\sigma_B k \\ M_C &= \left(\frac{16+37\kappa+21\kappa^2}{48} - \frac{6+16\kappa+11\kappa^2}{24}k\right)\frac{1}{(1+)\kappa^2} BD^2\sigma_B k \end{aligned}\right\} \quad (6)$$

where k is the distance between the extreme fiber in the compression side and the neutral axis, divided by the total depth D. With k changing from 0 to 1.0, *M–N* interaction curve for concrete is obtained, as plotted by thin solid line in Fig. 13 (a). Equation (6) is not valid when k exceeds 1.0. In this computation, the pure compressive strength (marked A on the interaction in Fig. 13 (a)) is assumed to be given by $0.75\sigma_B BD$, in other words, uniform strain $(1+\kappa)\cdot\varepsilon_B$ is distributed throughout the whole area.

b. *M–N* Interaction of H-Steel Section

The interaction of H-steel section may be obtained by connecting two extremums by a straight line; the full plastic states due to pure bending and uniaxial force. This interaction is a little conservative compared with the real interaction for H-steel cross section, however, for simplicity, the formula

$$\frac{M_s}{b\cdot t_f\cdot(1-2d_f)D\cdot{}_f\sigma_y + \frac{1}{4}t_w(1-2d_w)^2\cdot D^2{}_w\sigma_y} + \frac{N_s}{2b\cdot t_f\cdot{}_f\sigma_y + t_w(1-2d_w)\cdot D\cdot{}_w\sigma_y} = 1 \quad (7)$$

is taken for computing the interaction, and Eq. (7) is plotted in Fig. 13 (a) by a thin dashed line.

In Eq. (7),

M_s, N_s: bending moment and axial force (positive in compression) in H-steel, respectively.

${}_f\sigma_y$, ${}_w\sigma_y$: yield stresses of flange and web, respectively.

c. *M–N* Interaction of Main Reinforcing Bars

Interaction between bending moment M_r and axial force N_r (positive in com-

pression) of the main reinforcing bars can be obtained from

$$\frac{M_r}{a_{r_1}\cdot(1-2d_{r_1})\cdot D\cdot{}_r\sigma_{y_1}+a_r\cdot(1-2d_{r_2})\cdot D\cdot{}_r\sigma_{y_2}}+\frac{N_r}{2(a_{r_1}\cdot{}_r\sigma_{y_1}+a_{r_2}\cdot{}_r\sigma_{y_2})}=1 \quad (8)$$

where a_{ri}, ${}_r\sigma_{yi}$ and $d_{ri}D$ $(i=1, 2)$ are total area, yield stress and distance between the extreme fiber of the cross section and the gravity center of the bars, respectively (see Fig. 12). The results of computation by Eq. (8) is given by a thin dash-dotted line in Fig. 13 (a).

d. *M–N* Interaction of Total Cross Section

M–N interaction of the total cross section of steel reinforced concrete can be obtained as the maximum absolute value of the sum of vectors, which interpret the states of forces working on the concrete, H-steel and reinforcing bar cross sections. Results of computation for the *M–N* interaction of each specimen using the real dimensions of the column cross-section (tabulated in Table 5) are shown by thick solid lines in Figs. 13 (a) to (l). The interaction curve is symmetrical about the *N*-axis, and thus only a half portion (positive values for *M*) is shown in each figures.

Table 5. Dimensions of Cross Section.

Specimen	F1	F2	F3	F4	F5	F6
B	200.0	200.0	200.0	200.0	200.0	200.0
D	450.0	450.0	450.0	450.0	450.0	450.0
b	100.35	100.63	100.24	100.28	101.26	89.07
d	301.61	300.99	250.28	250.33	199.86	300.07
t_f	6.71	6.20	8.97	8.98	11.93	4.51
t_w	6.45	5.81	5.66	5.84	5.73	6.08
$d_f\cdot D$	77.55	77.61	104.34	104.33	131.04	77.22
$d_w\cdot D$	80.91	80.71	108.83	108.82	137.00	79.48
$d_{r1}\cdot D$	32.5	32.5	32.5	32.5	32.5	37.0
$d_{r2}\cdot D$						87.0
a_{r1}	2.54	2.54	2.54	2.54	2.54	3.98
a_{r2}						2.54
t_p	22.49	32.24	32.20	32.33	3.28	22.50
a	304.58	304.57	248.27	248.23	191.96	307.55
b	212.47	212.28	212.07	211.76	212.21	212.86

Specimen	F7	S1	S2	S3	R1	R2
B	200.0	200.0	200.0	200.0	200.0	200.0
D	450.0	450.0	450.0	450.0	450.0	450.0
b	99.87	101.34	100.24	90.00		
d	250.93	301.43	250.63	299.62		
t_f	6.03	6.66	8.99	4.48		
t_w	5.73	6.34	5.74	6.04		
$d_f\cdot D$	102.55	77.62	104.18	77.43		
$d_w\cdot D$	105.56	80.95	108.67	79.67		
$d_{r1}\cdot D$	34.0	32.5	32.5	34.0	38.5	38.5
$d_{r2}\cdot D$	84.0			84.0	88.5	88.5
a_{r1}	3.98	2.54	2.54	3.98	5.74	5.74
a_{r2}	2.54			2.54	5.74	5.74
t_p	32.30	6.41	5.83	6.55	22.54	32.28
a	254.86	304.55	248.67	307.22	300.00	299.5
b	211.99	211.52	212.39	212.90	212.86	212.58

Unit: mm

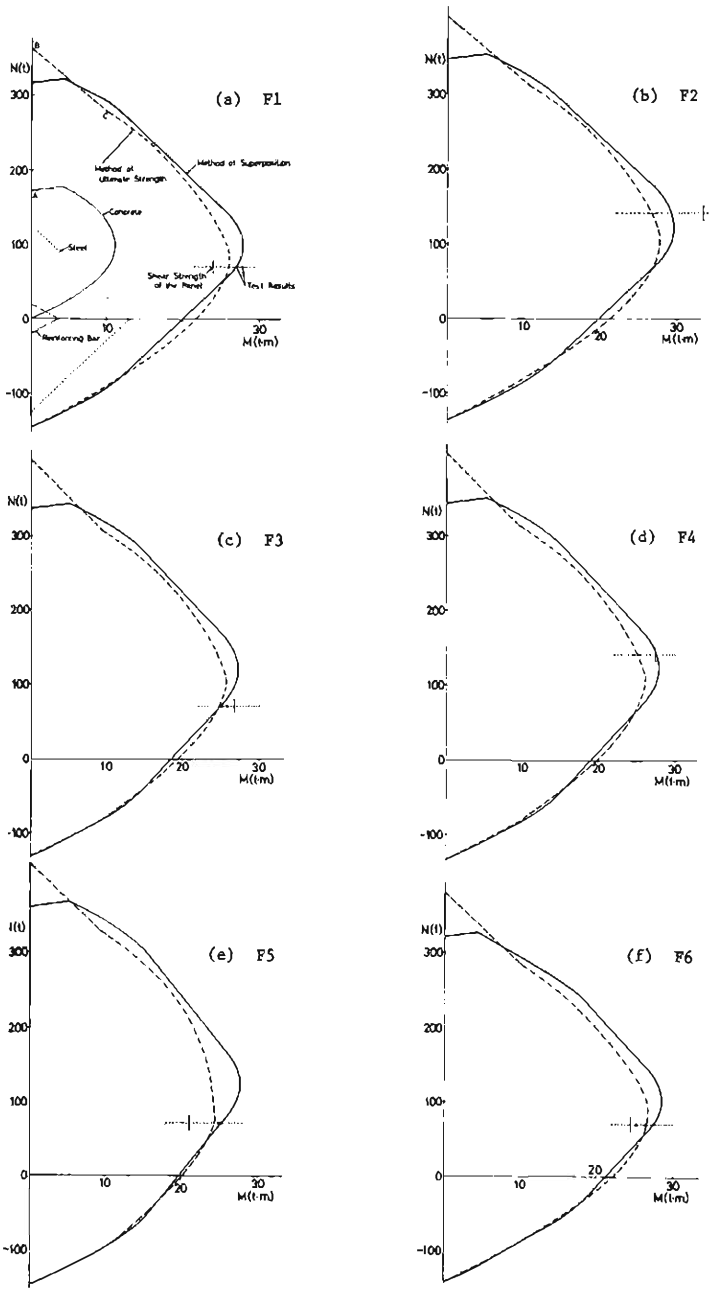

Fig. 13. Moment-axial force interactions.

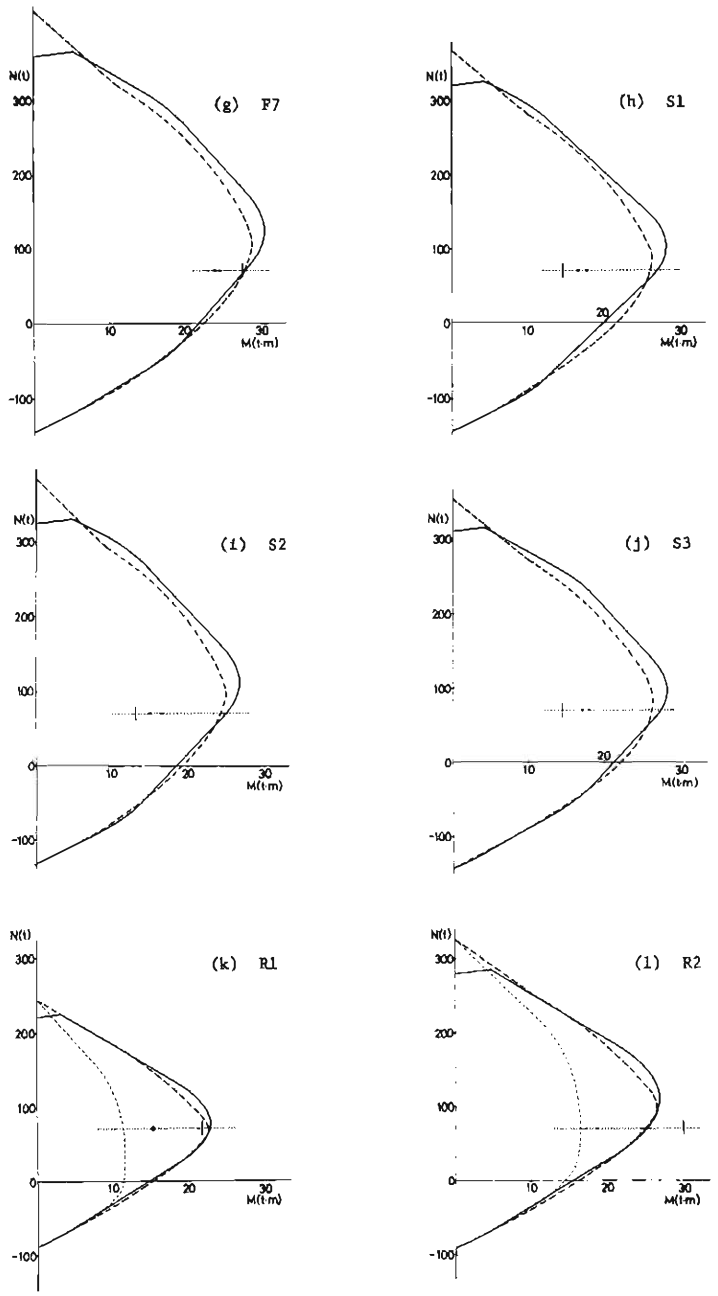

Fig. 13. Moment-axial force interactions (continued).

4.3 Maximum Flexural Strength of the Cross Section — Method of Ultimate Strength

As already described, this method assumes the linear variation of strains along the axis perpendicular to the axis of bending. One condition is that at the ultimate stage, the extreme fiber of the concrete in the compression side is subjected to $(1+\kappa)\varepsilon_B$.

a. M–N Interaction of Concrete

Interaction curve for concrete cross section is already given by Eq. (6) with an independent variable k.

b. M–N Interactions of Steel Flanges and Main Reinforcing Bars

As indicated in Fig. 14, strains in two flanges of H-steel; ε_1 and ε_2, are determined

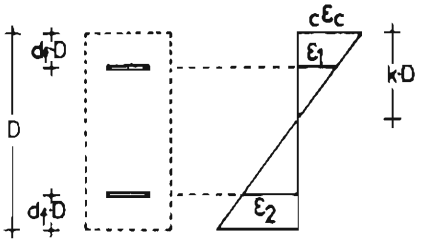

Fig. 14. Strains in flanges.

with a parameter k, taking two flanges as an ideal sandwich section. It is assumed that compression and tension are positive for ε_1 and ε_2, respectively. The axial force N_f (positive in compression) and bending moment M_f carried by two flanges are given by

$$\left.\begin{aligned} N_f &= b\cdot t_f\cdot {}_f\sigma_y\cdot(k_C-k_t) \\ M_f &= b\cdot t_f\cdot\left(\frac{1}{2}-d_f\right)\cdot D\cdot {}_f\sigma_y(k_C+k_t) \end{aligned}\right\} \tag{9}$$

where

$$\left.\begin{aligned} k_C &= \frac{k-d_f}{k}\cdot\frac{{}_c\varepsilon_C}{{}_f\varepsilon_y} \\ k_t &= \frac{1-d_f-k}{k}\cdot\frac{{}_c\varepsilon_C}{{}_f\varepsilon_y} \end{aligned}\right\} \tag{10}$$

${}_f\varepsilon_y$: yield strain of steel flanges $(={}_f\sigma_y/E)$

${}_c\varepsilon_C$: ultimate concrete strain $(=(1+\kappa)\varepsilon_B)$

E: Young's modulus of steel $(=2.1\times10^3\ \mathrm{t/cm^2})$

when the strains ε_1 and/or ε_2 exceed the yield strain $\pm{}_f\varepsilon_y$, Eq. (10) is not valid. Thus, the following limitation should be placed.

$$-1\le k_C\le 1 \text{ and } -1\le k_t\le 1 \tag{11}$$

In the case of the reinforcing bars, they can be treated as flanges of the ideal sandwich section. Therefore, the axial force N_{ri} (positive in compression) and bending

moment M_{ri} for the reinforcing bars in the first ($i=1$) and the second ($i=2$) rows can be readily computed from Eqs. (9), (10) and (11), by replacing N_f, M_f, $b\cdot t_f$, ${}_f\sigma_y$, ${}_f\varepsilon_y$ and d_f by N_{ri}, M_{ri}, a_{ri}, ${}_r\sigma_{yi}$, ${}_r\varepsilon_{yi}$ and d_{ri}, respectively. ${}_r\varepsilon_{yi}$ is the yield strain of the reinforcing bar, and is equal to ${}_r\sigma_{yi}/E$.

c. M–N Interaction of Steel Web.

The most complicated part in the method of ultimate strength is the computation for the interaction between the axial force N_w (positive in compression) and bending moment M_w carried by steel web. Refering to the strain distribution in the web, as shown in Fig. 15, only the results are presented here. Supposing that the compression is positive for ε_1 and the tension is positive for ε_2 and in addition that ${}_c\varepsilon_C > {}_w\varepsilon_y$, the following 6 cases are possible.

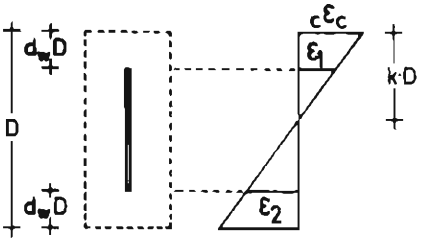

Fig. 15. Strain distribution in web.

Case 1: Both extreme fibers of the web yielding in tension.

$$\left.\begin{aligned} N_w &= t_w\cdot(1-2d_w)\cdot D\cdot {}_w\sigma_y \\ M_w &= 0 \end{aligned}\right\} \tag{12}$$

under the condition, $0 \le k \le \dfrac{d_w\cdot {}_c\varepsilon_C}{{}_c\varepsilon_C + {}_w\varepsilon_y}$ (13)

Case 2: Only the lower extreme fiber yielding in tension

$$\left.\begin{aligned} N_w &= t_w\cdot\left\{-(1-2d_w)+\frac{1}{2}\left(1+\frac{k-d_w}{k}\cdot\frac{{}_c\varepsilon_C}{{}_w\varepsilon_y}\right)\left(k-d_w+\frac{{}_w\varepsilon_y}{{}_c\varepsilon_C}k\right)\right\}\cdot D\cdot {}_w\sigma_y \\ M_w &= \frac{1}{12}t_w\left(1+\frac{k-d_w}{k}\cdot\frac{{}_c\varepsilon_C}{{}_w\varepsilon_y}\right)\left(k-d_w+\frac{{}_w\varepsilon_y}{{}_c\varepsilon_C}k\right)\left\{3-4d_w-2\left(1+\frac{{}_w\varepsilon_y}{{}_c\varepsilon_C}\right)k\right\}D^2\cdot {}_w\sigma_y \end{aligned}\right\} \tag{14}$$

under the condition,

$$\frac{d_w\cdot {}_c\varepsilon_C}{{}_c\varepsilon_C+{}_w\varepsilon_y} \le k \le \frac{d_w\cdot {}_c\varepsilon_C}{{}_c\varepsilon_C-{}_w\varepsilon_y} \text{ or } \frac{(1-d_w){}_c\varepsilon_C}{{}_c\varepsilon_C+{}_w\varepsilon_y} \tag{15}$$

Case 3: Both extreme fibers remaining elastic

$$\left.\begin{aligned} N_w &= \frac{1}{2}\cdot\frac{{}_c\varepsilon_C}{{}_w\varepsilon_y}\cdot t_w\cdot\frac{(1-2d_w)(2k-1)}{k}D\cdot\sigma_y \\ M_w &= \frac{1}{12}\cdot\frac{{}_c\varepsilon_C}{{}_w\varepsilon_y}\cdot t_w\cdot\frac{(1-2d_w)^3}{k}\cdot D^2\cdot {}_w\sigma_y \end{aligned}\right\} \tag{16}$$

under the condition,

$$\frac{(1-d_w)_c\varepsilon_C}{c\varepsilon_C+{}_w\varepsilon_y}\leq k\leq\frac{d_w\cdot{}_c\varepsilon_C}{c\varepsilon_C-{}_w\varepsilon_y} \tag{17}$$

Case 4: Only the upper extreme fiber yielding in compression

$$\left.\begin{aligned} N_w&=t_w\cdot\left[1-2d_w-\frac{1}{2}\left(1+\frac{1-d_w-k}{k}\cdot\frac{c\varepsilon_C}{{}_w\varepsilon_y}\right)\left\{1-d_w-\left(1-\frac{{}_w\varepsilon_y}{c\varepsilon_C}\right)k\right\}\right]\cdot D\cdot{}_w\sigma_y\\ M_w&=\frac{1}{12}\cdot t_w\cdot\left(1+\frac{1-d_w-k}{k}\cdot\frac{c\varepsilon_C}{{}_w\varepsilon_y}\right)\left\{1-d_w-\left(1-\frac{{}_w\varepsilon_y}{c\varepsilon_C}\right)k\right\}\\ &\qquad\left\{1-4d_w+2\left(1-\frac{{}_w\varepsilon_y}{c\varepsilon_C}\right)k\right\}\cdot D^2\cdot{}_w\sigma_y \end{aligned}\right\} \tag{18}$$

under the condition,

$$\frac{d_w\cdot{}_c\varepsilon_C}{c\varepsilon_C-{}_w\varepsilon_y}\ \text{or}\ \frac{(1-d_w)_c\varepsilon_C}{c\varepsilon_C+{}_w\varepsilon_y}\leq k\leq\frac{(1-d_w)_c\varepsilon_C}{c\varepsilon_C-{}_w\varepsilon_y} \tag{19}$$

Case 5: The upper extreme fiber yielding in compression, and the lower extreme fiber yielding in tension

$$\left.\begin{aligned} N_w&=t_w\cdot(2k-1)\cdot{}_w\sigma_y\\ M_w&=t_w\cdot\left\{(k-d_w)^2-\frac{1}{3}\left(\frac{{}_w\varepsilon_y}{c\varepsilon_C}\right)^2k^2+(1-2k)(k-d_w)\right\}D^2{}_w\sigma_y \end{aligned}\right\} \tag{20}$$

under the condition,

$$\frac{d_w\cdot{}_c\varepsilon_C}{c\varepsilon_C-{}_w\varepsilon_y}\leq k\leq\frac{(1-d_w)_c\varepsilon_C}{c\varepsilon_C+{}_w\varepsilon_y} \tag{21}$$

Case 6: Both extreme fibers yielding in compression

$$\left.\begin{aligned} N_w&=t_w(1-2d_w)\cdot D\cdot{}_w\sigma_y\\ M_w&=0 \end{aligned}\right\} \tag{22}$$

under the condition

$$\frac{(1-d_w)_c\varepsilon_C}{c\varepsilon_C-{}_w\varepsilon_y}\leq k\leq 1 \tag{23}$$

In the above equations, ${}_w\sigma_y$ and ${}_w\varepsilon_y$ is the yield stress and strain of web plate, respectively.

d. *M–N* Interaction of the Total Cross Section

From preceding sections a, b and c, *M–N* interaction relation for the total cross section is given by the summation

$$\left.\begin{aligned} N &= N_C + N_f + N_{r1} + N_{r2} + N_w \\ M &= M_C + M_f + M_{r1} + M_{r2} + M_w \end{aligned}\right\} \tag{24}$$

The results of computation for each specimen are shown by thick dashed lines in Figs. 13 (a) to (l). Since Eq. (6) is only valid when $0 \leq k \leq 1$, the interaction relation for the region $1 < k$ is given by a straight line connecting uniaxial loading case (point B in Fig. 13 (a)) and the point obtained under the condition, $k=1$ (point C in Fig. 13 (a). Under the uniaxial loading, N_0 is obtained assuming that the strain ε_y^{max} is uniformly distributed throughout the concrete cross section, where ε_y^{max} is the largest value among the yield strains of steel flange, web and the main reinforcing bars. It may be possible that the ultimate strength is given by negative value of k, when M is small, however, the computation is limited in the region where $0 \leq k \leq 1$.

4.4 Maximum Flexural Strength Considering the Bond Failure — Method of Ultimate Strength

The specimen R1 develops only 68% of the maximum horizontal load carrying capacity obtained from the maximum flexural strength of the column cross section. From the observations on the failure process and the crack pattern, it is noted that this strength reduction seen in specimen R1 is associated with the slip of the main reinforcing bars which are subjected to very steep stress gradient in the panel zone. It is considered that the bond failure occurs due to the insufficient bond length of the bars inside the connection panel. In order to investigate the states of normal stress in the bar and maximum bond stress in the panel zone, strain gauges are mounted at 10 discrete points of the bars in specimen R2 which are going straight through the panel zone. As shown in Fig. 7, 8 sets of 10 strain gauges are mounted on 4 reinforcing bars.

Figure 16 shows the change of the state of strain distributed along a bar in the first row. Each curve is drawn from the strain data at maximum load condition in each cycle indicated in the figure. The strain distribution is nearly antisymmetrical about the center line of the connection panel, when the maximum load (10 tons) is attained in 1/2 cycle of loading. After 2/2 cycle of loading, the tensile region of the bar in the panel gradually increases, and the tensile strain is distributed throughout the region of the bar inside the panel zone, at the maximum loads in 3/2 and 4/2 cycles of loading. At these states, the normal stress transmission is considered to be lost due to the bond failure. The strain distributions from the strain gauge data for the bars in the first and the second rows at the maximum load in 3/2 cycle of loading are shown in Figs. 17 (a) and (b), respectively. In Fig. 18, the mean values are plotted which are deduced from the curves in Fig. 17. The solid line is the strain distribution for the bars in the first row, and the dashed line is for those in the second row. The bond stress for the slipping reinforcing bars is computed from the stress gradient in the panel zone, which is determined based on the strain gradient given by straight dash-dotted line in Fig. 18. The so-determined bond stress ${}_b\tau_u$ is

$${}_b\tau_u = 36.49 \text{ kg/cm}^2 \tag{25}$$

The tensile and compressive forces in a bar in the column under antisymmetrical

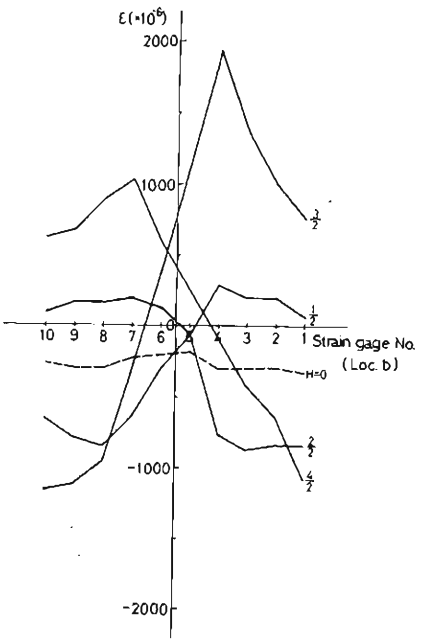

Fig. 16. Change of strain distribution in a reinforcing bar.

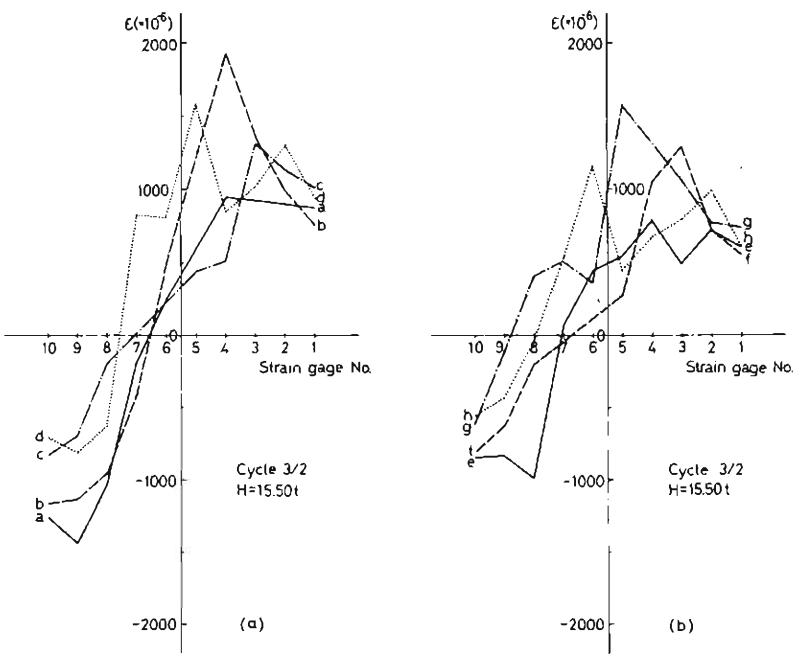

Fig. 17. Strain distributions in reinforcing bars.

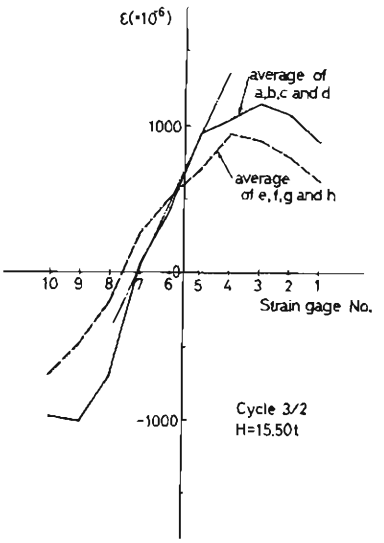

Fig. 18. Strain gradient in reinforcing bars.

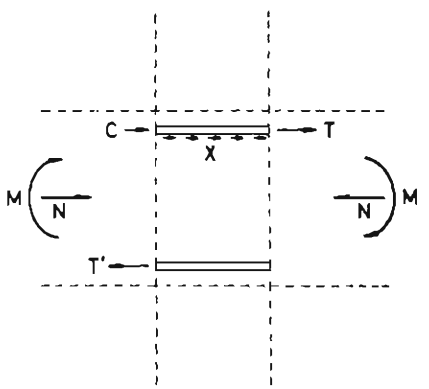

Fig. 19. Axial forces acting on reinforcing bars.

bending and axial force, are considered to act at both edges of the panel zone, as shown in Fig. 19. Defining these two forces to be T and C, the sum of T and C to be carried by the maximum bond strength

$$X = {}_b\tau_u \cdot \psi \cdot l_b \tag{26}$$

where

ψ: circumferential length of the bar

l_b: bond length (=30 cm; width of the panel zone)

Thus, $C + T \leq X$ (27)

In the actual computation, assuming that T is identical with the tension force oc-

curring in a bar in the tension side of the cross section, T' (see Fig. 19), Eq. (27) is considered in addition to Eq. (11). The results of computation for M–N interactions of column cross sections of specimens R1 and R2 are shown by thin dashed lines in Figs. 13 (k) and (l).

4.5 Maximum Shear Strength of the Connection Panel

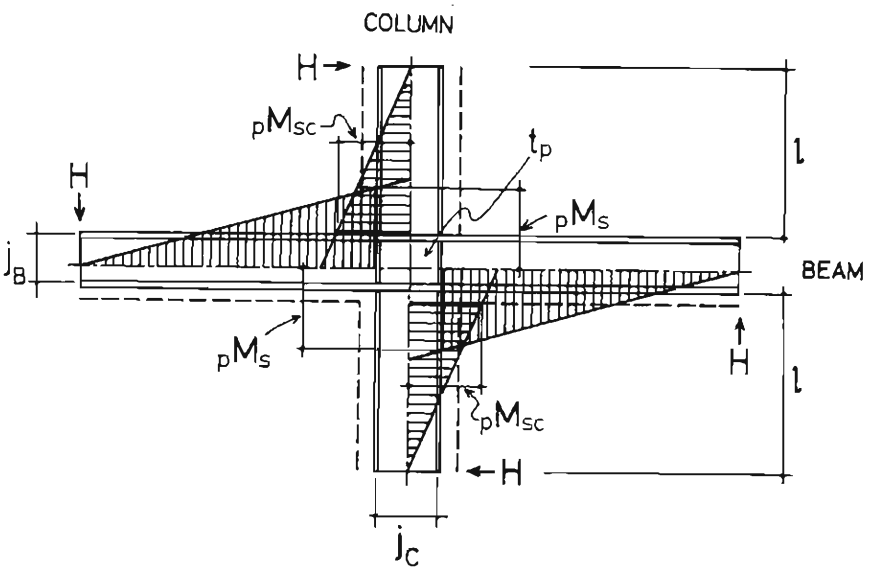

Fig. 20. Moment distribution in beam and column.

Referring to Fig. 20, the bending moment in the beam at the face of the steel flange, ${}_pM_s$, when the maximum shear strength of the connection panel is attained, is given by

$$ {}_pM_s = \frac{1}{2-\frac{j_B}{l}\alpha}({}_s\tau_w \cdot t_p \cdot j_B \cdot j_C + {}_c\tau_u \cdot j_B \cdot j_C) \tag{28} $$

Where

${}_s\tau_w$, ${}_c\tau_u$: maximum shear stresses of steel and concrete, respectively
j_B, j_C: Center-to-center distances of two flanges of the beam and column, respectively
B: mean value of widths of the beam and column
t_p: thickness of steel panel plate
l: clear length of the column
α: $={}_pM_{sC}/{}_pM_s$
${}_pM_{sC}$: the column moment at the beam face

In Eq. (28), the first and the second terms in the parenthesis indicate the contributions from steel and concrete to the maximum shear strength, respectively. The column moment ${}_pM_{sC}$ converted from ${}_pM_s$ in Eq. (28) for each specimen is indicated by

a vertical bar in Figs. 13 (a) to (l). The computation is carried based on

$$\left.\begin{aligned} \tau_w &= {}_p\sigma_y/\sqrt{3} \\ {}_C\tau_u &= 0.50F_C \end{aligned}\right\} \quad (29)$$

where ${}_p\sigma_y$ is the yield stress of the steel panel plate. The measured thickness of the panel plate, t_p, of each specimen is given in Table 5.

5. Discussions and Conclusions

Theoretical maximum horizontal load carrying capacities of each specimen based on the maximum flexural strength of the column cross section by the method of superposition and on the maximum shear strength of the connection panel are indicated in Figs. 8 and 9 by H_B and H_{ps}, respectively. Experimental maximum horizontal load carrying capacities attained in the positive and negative loading are converted to the column moment at the beam face, and plotted by the open and solid circles, respectively in Figs. 13 (a) to (l).

In Table 6, the theoretical and experimental load carrying capacities are summarized. Nomenclatures appearing in the table are as follows:

Table 6. Maximum Strength of specimen.

Specimen	F1	F2	F3	F4	F5	F6	F7	S1	S2	S3	R1	R2
H_{max}	26.0	25.5	24.1	23.6	23.5	24.8	22.9	16.6	15.5	16.8	12.8	15.5
H'_{max}	25.3	24.6	23.5	23.0	23.3	23.6	22.4	15.8	14.1	16.0	12.8	14.4
M_{max}	27.8	27.3	25.8	25.3	25.1	26.5	24.5	17.8	16.6	18.0	15.3	18.7
M'_{max}	27.0	26.3	25.1	24.6	24.9	25.3	23.9	16.7	15.1	17.1	15.3	17.3
M_B	26.9	29.3	24.9	27.6	25.2	27.3	27.8	27.1	24.9	27.3	22.7	25.2
M'_B	26.0	26.8	24.7	25.1	24.3	26.6	27.8	26.2	24.3	26.2	22.6	25.0
M''_B											11.4	16.5
${}_pM_{sc}$	24.0	33.4	26.7	27.4	21.1	24.5	27.5	14.7	13.2	14.5	21.7	29.9
H_B	25.2	27.4	23.3	25.8	23.6	25.5	26.0	25.3	23.3	25.5	18.9	20.9
H'_B	24.3	25.1	23.1	23.5	22.7	24.9	26.0	24.5	22.7	24.5	18.8	20.8
H''_B											9.5	13.7
H_{ps}	22.4	31.23	25.0	25.3	19.7	22.9	25.7	13.7	12.4	13.5	18.0	24.9

Unit is ton and t·m for the load and bending moment, respectively.

Experimental strength:

H_{max}: maximum horizontal load in the positive loading

H'_{max}: maximum horizontal load in the negative loading

M_{max} M'_{max}: the column moment at the beam face based on H_{max} and H'_{max}, respectively

Theoretical strength:

M_B: maximum flexural strength of the column by the method of superposition

M'_B: maximum flexural strength of the column by the method of ultimate strength

M''_B: maximum flexural strength of the column by the method of ultimate strength considering the bond failure

${}_pM_{sc}$: the column moment when the maximum shear strength of the connection panel is attained

H_B, H'_B, H''_B, H_{ps}: the horizontal load based on M_B, M'_B, M''_B and ${}_pM_{sc}$, respectively

5.1 *M–N* Interaction

Two types of M–N interactions, based on the methods of superposition and ultimate strength show reasonable agreement. At the two extreme cases, pure compression and pure bending, discrepancy becomes large. The discrepancy in the pure compressive strengths is considered due to the deference of the stress distribution assumed in both methods. M–N interaction for H-steel section is accurately computed in the method of ultimate strength, while that is approximated by a straight line in the method of superposition (Eq. 7). This causes the discrepancy in the M–N interactions obtained by two methods for the total cross section around the region of pure bending.

In general, at the level of the compression load 70 tons, the bending moments given by both methods are nearly equal, and they fairly well estimate the maximum horizontal load carrying capacities of specimens failing in the flexure of the column cross section, except for specimens F7, R1 and R2, whose cases are discussed later.

When the axial load becomes 140 tons, discrepancy between two interactions becomes large, and the flexural strength given by the method of ultimate strength (shown by dashed line in each of Figs. 8 (b), (d), 9(b) and (d)) gives better estimation to the experimental load carrying capacity.

In case of F7, the identical maximum horizontal load carrying capacity is obtained both from the methods of superposition and ultimate strength. However, the experimental result shows quite large discrepancy with the theoretical one. Since the theoretical result for the maximum strength of specimen F5, which has the smallest depth of H-steel, shows good agreement with the experimental result, the discrepancy seen in case of F7 cannot be considered to be caused only due to the large difference between the depth of H-steel and the total depth of the cross section. It is considered that the slip of the reinforcing bars causes the strength reduction, as seen in specimens R1 and R2.

Based on the maximum bond stress given by Eq. (25), which is experimentally detected, the maximum load carrying capacity is computed for specimen R2 in section 4.4. Although some unrealistic assumptions are made, such as the constant bond capacity (X in Eq. (27)) and non-compatibility of the strain in the bar, in which the stress is limited by X, with the strain in concrete, the result of the computation happens to be of a good agreement with the experimental result. Assuming the ratio of the maximum bond stress ${}_b\tau_u$ to the cylinder strength F_c is constant, the analysis is also carried for specimen R1, and the result is shown by dashed line in Figs. 8 (k) and 9 (k). In this case, the discrepancy between the theoretical and experimental maximum load carrying capacities is very large. And thus, the refined analysis for the bond strength is needed.

5.2 Maximum Shear Strength of the Connection Panel

The maximum load carrying capacities computed from the maximum shear strengths of the connection panel, which are described in Sect. 4.5, are based on the maximum shear stress given in Eq. (29). The shear failing specimens, S1, S2 and S3, exceed the corresponding theoretical maximum load carrying capacities. On the other hand, for specimens F1, F5, F6 and F7, the maximum load carrying capacities based on the shear failure of the panel are much less than those computed from the maximum flexural strength of the column. Since the theoretical maximum load carrying capacities of those specimens are attained in the test, it cannot be directly concluded that the shear failure occurs, although the yielding in the panel is quite obvious. It is rather reasonable to conclude that the assumed maximum shear stress is too conservative. In case of specimen F5, very small concrete volume assumed to resist the shear in the analysis results in the low load carrying capacity.

Solid line in Fig. 21 is obtained by connecting the origin and maximum load points in the first loading cycles at each displacement amplitude, for specimen S1. The plateau of the dashed line gives the load converted from the contribution by the

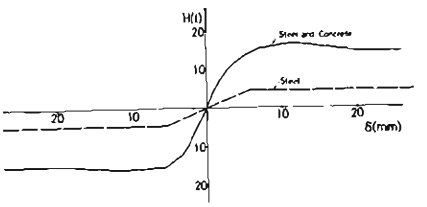

Fig. 21. Horizontal load-displacement curve of S1.

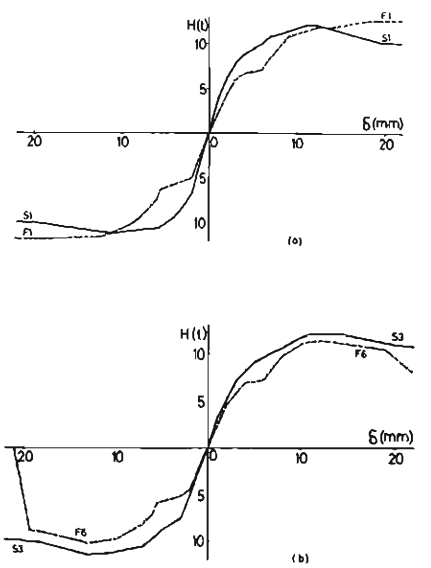

Fig. 22. Shear strength of concrete in connection panel.

steel panel to the maximum shear strength. The elastic portion of the dashed line is drawn by connecting the origin and the point at which the strain data of the rosette gauges detected in the test begin to increase at a high rate. From the similar load-displacement curves for specimen F1, F6 and S3, the differences between the solid and dashed lines are summarized in Figs. 22 (a) and (b). These curves are considered to be the contributions from the concrete to the strength of the connection panel. From these figures, it is observed that the contribution due to the concrete is larger in the shear failing specimen than in the corresponding flexure failing one*9, and thus it can be said that the connection panel of the flexure failing specimen has not yet failed. The mean value of the maximum shear stress computed from the curves for specimen S1 and S3 in Fig. 22, is as follows; as the maximum value, ${}_c\tau_u=0.649F_c$, and at the yielding of the steel plate, ${}_c\tau_u=0.541F_c$.

5.3 The Effect of Axial Force

The test results of specimens F2 and F4 show that the theoretical maximum load carrying capacity can be attained even when the vertical load becomes large, since the P–Δ effect could be neglected at the column end at the beam face in the present testing system. It is already pointed that the experimental strength is lower than the prediction by the method of superposition.

The effect of the large axial force appears in the strength deterioration due to the repetition of the loading and the small deformation capacity. The tests are terminated when it becomes impossible to keep the vertical load constant because of the rapid increase of the out-of-plane deformation.

5.4 Effect of H-Steel Depth and Flexural Ratio

As long as the present test results are concerned, it seems that no problem is caused when the depth of the H-steel section is reduced, the flexural ratio being kept to be 0.8. The maximum load carrying capacity can be well predicted by the corresponding analysis to the failure mechanism. When the flexural ratio becomes 0.4, the maximum flexural strength of column cross section can be developed as seen in the test result of F6. However, that of F7 cannot be attained because of the slip of the reinforcing bars. In case of the flexural ratio of 0, i.e., the ordinary reinforced concrete column, the problem of the slip of the reinforcing bars is already indicated.

The undesired deterioration of the strength and the energy dissipation capacity are not observed from the test results. It should be pointed out that the method of analysis for the maximum shear strength of the connection panel, presented in Sect. 4.5, cannot give a very good estimation to the real strength of the specimen, when the depth of the H-steel section becomes very small, since the concrete volume enclosed in flanges of the beam and column is assumed to resist to the shear in the analysis.

It seems that the combination of the small flexural ratio and small depth of H-steel section may cause a problem. This implication is derived from the fact that

*9: In the large displacement range, the curve for F1 exceeds that for S1, because of the strain-hardening of steel. The steep unloading curve in specimen F6 is caused by the breakage of the welded column end.

of the discrepancy between the maximum experimental and theoretical load carrying capacities of specimen F7 is quite similar to those of specimens R1 and R2, whose flexural ratio is zero. The slip of the reinforcing bars may have also occurred in specimen F7.

5.5 Conclusions

1. The maximum flexural strength of the steel reinforced concrete cross section is well predicted by the method of superposition.
2. The prediction of the maximum shear strength of the connection panel largely depends on the assumed value of the maximum shear stress and the size of the concrete volume assumed to resist the shear.
3. When the ordinary reinforced concrete column is combined with the pure steel concrete beam, the slip of the reinforcing bars causes the large strength reduction and the deterioration of the energy dissipation capacity. The more refined analysis based on the real stress transmission pattern in the connection panel is needed.
4. The specimen under large vertical load could sustain the theoretical maximum load. However, the strength deterioration and the reduction of the deformation capacity are critical, compared with the corresponding specimens under the smaller vertical load.
5. The shape of the hysteresis loop of the specimens with steel reinforced column is a typical spindle type. The hysteresis loop of the shear failing specimen in the connection panel is slightly thinner than that of the flexure failing specimen in the column. In case of specimen with ordinary reinforced concrete column, the energy dissipation capacity is not much expected.
6. The share by the H-steel section to the flexural strength of the total cross section can be partly replaced by the reinforcing bars, within the limitation of the results of the present test series.

Acknowledgements

The work presented in this paper has been financially supported by Japan Housing Corporation and Takenaka Komuten Co. Ltd.. The man power needed for conducting the tests were supplied by Takenaka Komuten. The authors would like to present sincere appreciation for their support.

Acknowledgements are also due Messrs M. Sano, E. Akiyama and T. Sakai, who were the students in Osaka Institute of Technology, and N. Yoshida, the student of Kyoto University. They helped the preparation of the manuscript of this paper.

References

1) Wakabayashi, M., S. Takada and H. Saito: Steel Reinforced Concrete Structures, Structural Engineering Series (Kenchiku Kozogaku Taikei), Vol. 19, 1967, Shokokusha (Tokyo), 32–72 (in Japanese).
2) Wakabayashi, M., et al.: Steel Reinforced Concrete Structures, Architectural Engineering Series (Kenchikugaku Taikei), Vol. 18, 1970, Shokokusha (Tokyo), 242–273 (in Japanese).